Scattering cross sections for collisions of electrons with tetrahedral molecules in the energy range 0.1–100 eV: CH_4, SiH_4, and GeH_4

Mandeep Kaur,[1,2] Gurpreet Kaur,[1] Arvind Kumar Jain,[1] Harsh Mohan,[1] Parjit S. Singh,[2] Sunita Sharma,[3] and K. L. Baluja[4,*]

[1]*Department of Physics, M.L.N. College, Yamuna Nagar, 135 001, Haryana, India*

[2]*Department of Physics, Punjabi University, Patiala, 147 002, Punjab, India*

[3]*Department of Chemistry, M.L.N. College, Yamuna Nagar, 135 001, Haryana, India*

[4]*Department of Physics and Astrophysics, University of Delhi, Delhi, 110 007, India*

(Received 15 March 2018; published 30 May 2018)

The impact of electron interaction with CH_4, SiH_4, and GeH_4 molecules (i.e., tetrahedral molecules) is described here to calculate elastic differential, integral, and momentum-transfer cross sections as well as total (elastic plus inelastic) cross sections using a parameter-free spherical complex optical potential approach in the fixed nuclei approximation at energies from 0.1 to 100 eV. The optical potential is constructed from a near-Hartree-Fock one-center expansion of projectile-target interaction wave function. We demonstrate that the qualitative features of the scattering parameters [such as a Ramsauer-Townsend (RT) minimum and shape resonance] as observed in recent experiments, are very well reproduced in the present spherical model. The value of the RT minimum has been correlated with the scattering length to the dipole polarizability of the target molecule. The calculated cross sections are compared with available theoretical calculations and experimental measurements in this energy region.

DOI: 10.1103/PhysRevA.97.052711

I. INTRODUCTION

The collision studies of low-energy electrons with tetrahedral molecules like methane (CH_4) and silane (SiH_4) have attracted significant interest in various fields. In scientific fields, finding a high-temperature superconductor has been one of the important issues in the last few years. The hydrogen-rich compounds, especially the hydrides of group IV, are expected to be high-temperature superconductors for comprehending the superconductivity of metallic hydrogen. This attracted more attention for the hydrides of group IV like SiH_4, CH_4, and GeH_4 [1,2]. Germane is used in the semiconductor industry for the epitaxial growth of germanium by MOVPE or chemical beam epitaxy because of its thermal instability at high temperature [3]. Further, highly purified silane gas is required for manufacturing of advanced silicon semiconductor devices [4]. Apart from the semiconductor industry, there has been considerable interest in applications of low-temperature plasma technology, particularly in the field of the nano- and optoelectronic industries. For deposition of high-quality Si-C-H film, the plasma decomposition of gas mixtures of silane and methane is often employed [5]. Various studies are needed to understand the physics that arise in such low-temperature plasma. The mechanism at these low temperatures has complicated processes which require the knowledge of electron-molecule collision cross sections. In view of this, significant attention has been paid to the electron-molecule collision from very low to intermediate electron impact energies in laboratory as well as in theory. Let us now briefly discuss the status of the experimental and theoretical research on the scattering of electrons with methane, silane, and germane molecules and the purpose of carrying out the present calculations.

Recently, Song *et al.* [6] have represented the "recommended" values of the total scattering, elastic scattering, momentum transfer, excitations of rotational and vibrational states, dissociation, ionization, and dissociative attachment cross sections for electron collisions with methane in the energy range 0.001–4000 eV. Apart from this, a lot of experimental and theoretical data is available for various types of cross sections for electron impact on T_d molecules. On the experimental side, the main techniques used are the time-of-flight technique [7–10], crossed electron-beam spectrometer technique [11–16], linear electron-transmission method [17–22], Boltzmann equation along with Monte Carlo simulation method [23], and relative flow method [24].

From a theoretical perspective, four different models have computed the cross sections for electron impact on molecules studied here. The independent atom model (IAM) has been widely used to compute cross sections for electron collision with various polyatomic molecules. The main advantage of this method is that molecular cross sections are the coherent sum of the atomic cross sections constituting the molecule. This method has a serious drawback because it neglects the chemical bonding effect of the atoms. This method works at high energies because the screening effects become less significant. However, the IAM enjoys its popularity due to its economy in computational work. This method is suitable for molecules which have more or less spherical symmetry. Mozejko *et al.* [25] used this method for T_d molecules like SiH_4 and GeH_4.

One of the most widely used theoretical methods to compute electron impact cross sections for molecules is the *R*-matrix

*Present address: Department of Physics and Astrophysics (retired), University of Delhi, Delhi, 110 007, India.

method [26,27]. This is an *ab initio* method based on the variational principal. The efficiency of this method arises due to the partitioning of the configuration space into an inner region and outer region. The inner region is chosen in such a way that it envelops the entire charge cloud of the molecule. In this region multicenter integrals are involved but these are solved analytically by employing Gaussian-type orbitals for bound and scattering electrons. The main advantage of this method is that a large number of cross sections over a fine energy grid can be calculated. The main drawback is about balancing the correlation effects in the target and target plus scattering electron system. Pseudoresonances, which are an unphysical feature, also appear above the last excitation threshold included in the calculation.

Several calculations have been performed by using the Schwinger multichannel (SMC) method at various levels of approximation [28–34]. SMC method is an *ab initio* variational method and takes into account the complexities that arise in scattering involving many-particle systems. An important feature is that all required matrix elements are independent of the long-range behavior of the trial functions. The main advantage of this method is that it includes arbitrary boundary conditions through the Green's function. However, for large molecules many basis functions are necessary for convergence of the cross sections. In sharp contrast to the R matrix, the scattering calculations have to be repeated at each energy. Another drawback of this method is the heavy computation efforts in calculating the Green function matrix elements.

The spherical complex optical potential (SCOP) model has been quite successful in the evaluation of cross sections for polyatomic molecules [35–44]. In the SCOP model, all the potentials are localized, which makes it suitable for efficient computation. The total potential consists of real potentials like the static, the exchange, and the polarization along with an imaginary potential that represents inelastic effects. This method is suitable for energies above ionization threshold for nonspherical polyatomic molecules. We expect this method to work for T_d molecules that are nearly spherical, which do not possess dipole and quadrupole moments. Here, the only nonvanishing multipole moment is the octupole moment. Its contribution is negligibly small. The main limitation of this method is that it does not yield excitation and ionization cross sections separately. Jain *et al.* [41] have carried out calculations for the germane molecule using Hara free-electron gas exchange and correlation polarization interactions, but they have not included the effect of the absorption potential. They also confirmed the existence of shape resonance at around 5 eV. It is worth mentioning here that the observed features such as Ramsauer-Townsend (RT) minimum and shape resonance in the integral and momentum-transfer cross sections are very sensitive to the choice of various model potentials (exchange and polarization). This is one of the goals of the present study, i.e., to test how good the modified semiclassical exchange potential is along with the parameter-free correlation polarization potential in order to give the RT effect at low energies and a shape resonance phenomenon at further high energies.

The RT effect is a purely quantum mechanical effect that occurs when the projectile effectively sees a transparent target. Quantitatively speaking, an s-partial wave gets diffracted around the target molecule and is distorted by the attractive polarization potential so strongly that the incoming wave is pulled in by a factor of π rad in the phase shift. This gives rise to a minimum in the cross section. The cross section does not drop to zero because of slight contamination by higher partial waves. This effect is predominantly observed in molecular targets of higher polarizability like CH_4 but is not observed in its isoelectronic neon which has polarizability almost an order of magnitude smaller than CH_4.

Below the first excitation threshold, we observe the shape resonances in all the molecules that occur when the projectile tunnels through the centrifugal barrier $\ell(\ell+1)/r^2$, where ℓ is the angular momentum of the ℓth partial wave. From the chemical point of view the incoming electron occupies the virtual lowest unoccupied molecular orbital (LUMO) that has positive energy. This positive energy is very close to the resonance position of the shape resonance.

Another goal of this paper is to study the role of the absorption potential with respect to the experimental measurements. Since these molecules have no dipole and quadrupole moments, we therefore assume these molecules to be spherical. This is a very good approximation for computational reasons in order to avoid nonspherical terms in the potential. Therefore, all the terms included in the optical potential are spherical. This spherical model has earlier been tested in detail for the SiH_4 molecule in the low-energy region (Jain *et al.*, [42]). The SiH_4 and GeH_4 molecules present a stringent test for the validity of the spherical model of a very complicated and highly polarizable target. Keeping this in mind, we have calculated the elastic differential, integral, and momentum-transfer cross sections along with total (elastic plus inelastic) cross sections for the scattering of electrons with CH_4, SiH_4, and GeH_4 molecules using the SCOP model.

Further, from a structural standpoint, these three molecules belong to the same T_d point group; however, the SiH_4 and GeH_4 systems have a large electronic configuration and a much higher polarizability than the CH_4 molecule. It is therefore interesting to study the collision of electrons with these molecules in this energy region.

In the past, several local prescriptions have been developed to model exchange and polarization forces (see review by Gianturco and Jain [44], for more details) with the goal in mind that the model potentials be free from adjustable parameters. The use of a correlation polarization potential (originally derived by O'Connell and Lane [45] for electron-atom scattering and later modified by Padial and Norcross [46] for electron-molecule cases) has been found quite promising. For exchange interaction, the modified semiclassical exchange (see, for example, Gianturco and Scialla [47]) has been used in the present study.

II. THEORETICAL METHODOLOGY

All the three molecules, i.e., CH_4, SiH_4, and GeH_4, belong to the T_d symmetry point group (electronic $^1A_1$ ground state) with the electronic configuration $1a_1^2 2a_1^2 1t_2^6$ [48], $1a_1^2 2a_1^2 1t_2^6 3a_1^2 2t_2^6$ [49], and $1a_1^2 2a_1^2 1t_2^6 3a_1^2 2t_2^6 1e^4 3t_2^6 4a_1^2 4t_2^6$ [41], respectively. A single-center expansion technique (see Gianturco and Thompson [50]) with carbon, silicon, and germanium atoms at the center is employed for all orbitals in the near-Hartree-Fock limit using experimental values of

nuclear geometry (bond length = 1.085 Å and bond angle = 109.5° for CH_4; bond length = 1.480 Å and bond angle = 109.45° for SiH_4; bond length = 1.527 Å and bond angle = 109.4° for GeH_4). The pivotal quantity in the calculations of optical potential is the charge density $\rho(\vec{r})$ which is calculated from the single-center wave function with a large number of terms in the expansion of each bound orbital (for details, see Ref. [38]). The $\rho(\vec{r})$ is then expanded in terms of the symmetric A_1 irreducible representation of the molecular C_{3v} point group, i.e.,

$$\rho(\vec{r}) = \sum \bar{\rho}_{\rm LH}(\vec{r}) X^{A_1}_{\rm LH}(\hat{r}). \quad (1)$$

In the spherical approximation [39,40], only the first term ($L = 0$, $H = 1$) of the expansion of Eq. (1) is needed in order to evaluate all the three local potentials, namely, the static ($V_{\rm st}$), the exchange ($V_{\rm ex}$), and the polarization ($V_{\rm pol}$). An explicit expression for $V_{\rm st}(\vec{r})$ is given in the literature (see, for example, Gianturco and Jain [44]). The detailed expression for the modified semiclassical exchange (MSCE) can be seen in our earlier publication [43]. According to O'Connell and Lane [45], the correlation polarization potential is obtained in the whole radial region by smoothly joining the correlation energy function and the asymptotic form $-\alpha_o/2r^4$ (α_o, the dipole polarizability for CH_4 is 17.50 a_0^3 [35], for SiH_4 is 31.90 a_0^3 [49], and for GeH_4 is 44.353 a_0^3 [41]), where they cross each other for the first time (the crossing point occurs at 3.96 a_0 for CH_4, 4.49 a_0 for SiH_4, and 5.3 a_0 for GeH_4). The functional form of the correlation polarization potential in the inner region of the interaction is derived from an approximate local correlation energy which is obtained in terms of charge density $\rho(\vec{r})$ following Padial and Norcross [46] and Gianturco *et al.* [51].

Furthermore, the imaginary part of the optical potential (i.e., $V_{\rm abs}$) is also used to include the combined effect of all the inelastic channels. An improved version of the absorption potential as discussed by Blanco and Garcia [52] is employed here. The details are given in our earlier publication [43]. In this potential, we have fixed the value of Δ (free parameter) equal to the threshold energy for the first electronic excitation of the target molecule. In the present calculations, the experimental value of Δ is taken as 10.9 eV for CH_4 [48], 8.7 eV for SiH_4 [48], and 7.5 eV for GeH_4 molecule [24].

Finally, a partial wave analysis approach is adopted to compute the lth partial wave phase shifts for the solution of the following radial Schrödinger equation.

$$\left[\left(\frac{d^2}{dr^2}\right) + k^2 - \frac{l(l+1)}{r^2} - V_{\rm opt}(\vec{r})\right] f_l(k\vec{r}) = 0. \quad (2)$$

We employ the variable-phase approach (VPA) [53] to find the solution of the above equation. The corresponding quantities, elastic differential cross section (DCS), integral cross section ($\sigma_{\rm el}$), and momentum-transfer cross section (σ_m), along with total (elastic plus inelastic) cross section (σ_t) are then easily obtained from the S matrix at each energy. All our cross sections have converged with respect to the number of partial waves.

III. RESULTS AND DISCUSSION

A. Electron scattering from methane, CH_4

In this paper, we present elastic differential cross sections (DCSs) only at those energies where both experimental as well as other theoretical results are available. Therefore, in Figs. 1(a)–1(f), DCSs of the $e-CH_4$ system are displayed at energies of 5, 7.5, 10, 15, 20, and 30 eV, respectively. It should be noted in general that in the present fixed nuclei approximation, the DCS at $\theta = 0°$ are not defined; therefore the zero-angle points in these figures should not be taken seriously. The experimental DCSs of Boesten and Tanaka [14] are available at all of these energies whereas the measurements of Tanaka *et al.* [13] are available at all energies except at 30 eV. Also, the measurements of Cho *et al.* [11] and recommended values of Song *et al.* [6] are available at energies of 5, 10, 20, and 30 eV. Further, Sohn *et al.* [15] measured the DCSs at 5 eV only and the results of Curry *et al.* [12] are available at 7.5, 10, 15, and 20 eV. We also compare our DCSs with the theoretical calculations of Cho *et al.* [11], Nestmann *et al.* [27], Bettega *et al.* [28,29], Lima *et al.* [32,33], and Jain [36].

In Fig. 1(a) the DCSs are presented at an energy of 5 eV. The shape of the DCS appears due to the dominance of d-wave scattering. It is described by two forward and backward peaks with two minima at 40° and 120°. The present results are in good agreement with the recommended values of Song *et al.* [6] and the measurements of Cho *et al.* [11] up to 40°; thereafter between 40° and 80° our results are slightly higher. Beyond 80° our DCS agrees well with the values of Song *et al.* [6] at all available angles, whereas the present DCS agrees well with the measurements of Cho *et al.* [11] up to 110°. Thereafter, the measurements of Cho *et al.* [11] are not in agreement with any calculation or measurements. The dip position in the cross section at 120° is in good agreement with the experimentally measured values [13,15] as well as the recommended values of Song *et al.* [6]. At 7.5 eV [Fig. 1(b)], our results are in good agreement with the experimental as well as theoretical calculations in the entire angular region except at lower angles where the present results are a bit higher due to fixed nuclei approximation. In Fig. 1(c), the DCSs are plotted at an energy of 10 eV. The present results agree well with the experimental measurements between 30° and 90°. Thereafter a dip arises at 110° which is at a similar position as that of Lima *et al.* [32]. However, at a scattering angle $\theta \geqslant 130°$, the present results agree well with the calculations of Bettega *et al.* [29] and Lima *et al.* [32], whereas the measurements of Cho *et al.* [11] are lower and the difference increases with increase in scattering angle in backward scattering. The trend is continued for other higher energies, i.e., 15 and 20 eV [see Figs. 1(d) and 1(e), respectively]. In continuation to this DCSs are also plotted at an energy of 30 eV [Fig. 1(f)]; the present calculations reproduce well the recommended values of Song *et al.* [6] between 30° and 60°. Thereafter the present results are a bit lower as compared to other results accompanied with a dip at 100°.

At the low-impact-energy region ($E < 1$ eV), study of total cross sections for the scattering of electrons with any atom or molecule is very interesting, particularly if they are able to demonstrate the RT minima. In view of this, we have calculated elastic integral cross sections ($\sigma_{\rm el}$) as well as

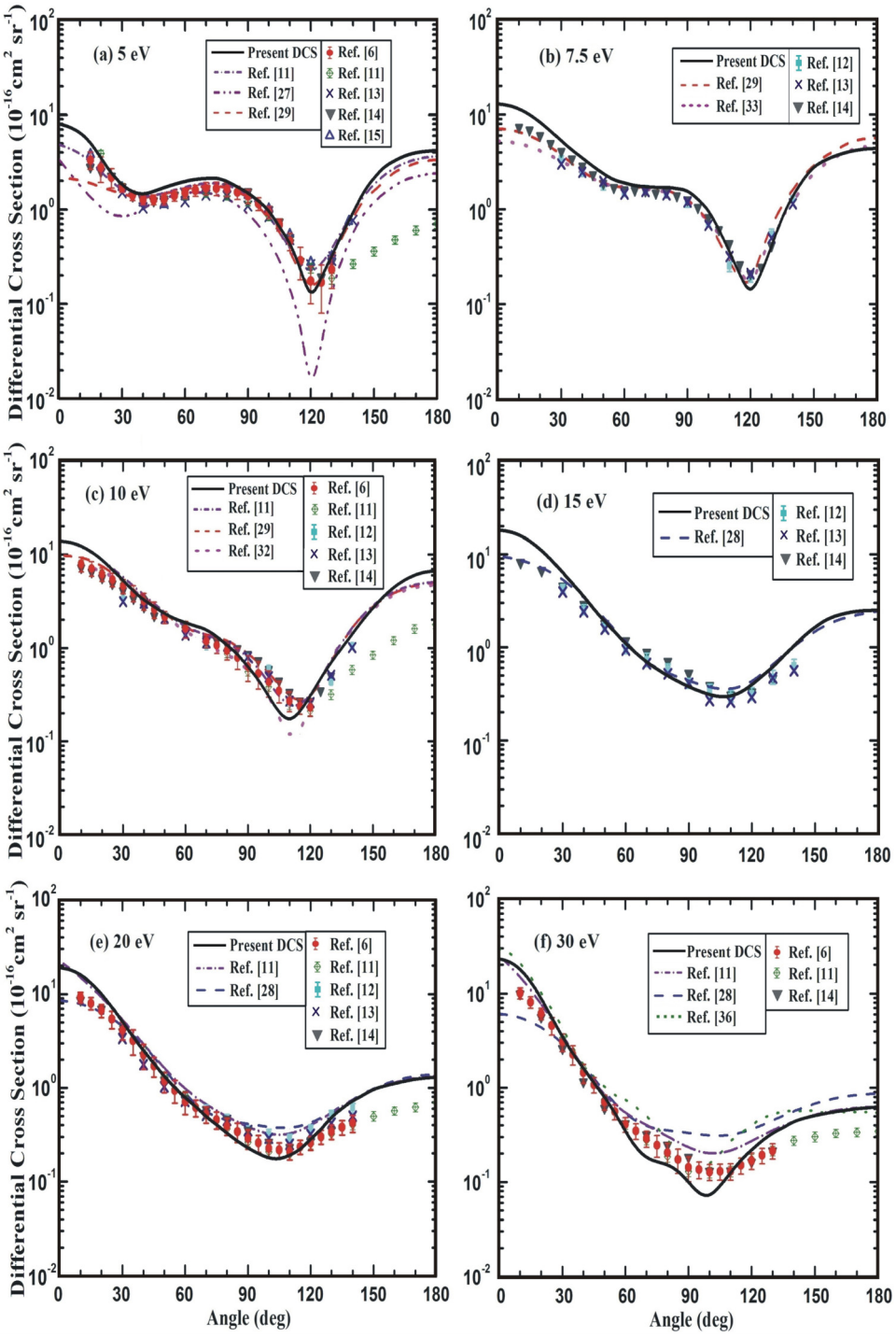

FIG. 1. Differential cross sections for $e-CH_4$ scattering at energies (a) 5, (b) 7.5, (c) 10, (d) 15, (e) 20, and (f) 30 eV. Present results: Black solid line, elastic DCS. Other calculations: Violet short dashed-dot line, Cho *et al.* [11]; purple dashed-dot-dot line, Nestmann *et al.* [27]; blue dashed line, Bettega *et al.* [28]; red dashed line, Bettega *et al.* [29]; violet big dotted line, Lima *et al.* [32]; magenta big dotted line, Lima *et al.* [33]; olive dotted line, Jain [36]. Experimental data: Red filled circle, Song *et al.* [6]; olive diamond with plus, Cho *et al.* [11]; cyan filled square, Curry *et al.* [12]; royal cross, Tanaka *et al.* [13]; dark gray inverted filled triangle, Boesten and Tanaka [14]; blue hollow triangle, Sohn *et al.* [15].

total (elastic plus inelastic) cross sections (σ_t) in the energy range 0.1–100 eV and compared the present results with the recent recommended values of Song *et al.* [6] along with other measurements [7,9,11,14,17] in Figs. 2(a) and 2(b). The calculations of Cho *et al.* [11], Vinodkumar *et al.* [26], and Bettega *et al.* [28,29] are also presented in these figures. In Fig. 2(a), cross sections are presented up to 20 eV. The corresponding data below 1 eV are also shown in the inset of this figure. Before we discuss our results, we would like to point out that only in the lower-energy region (i.e., <20 eV), the

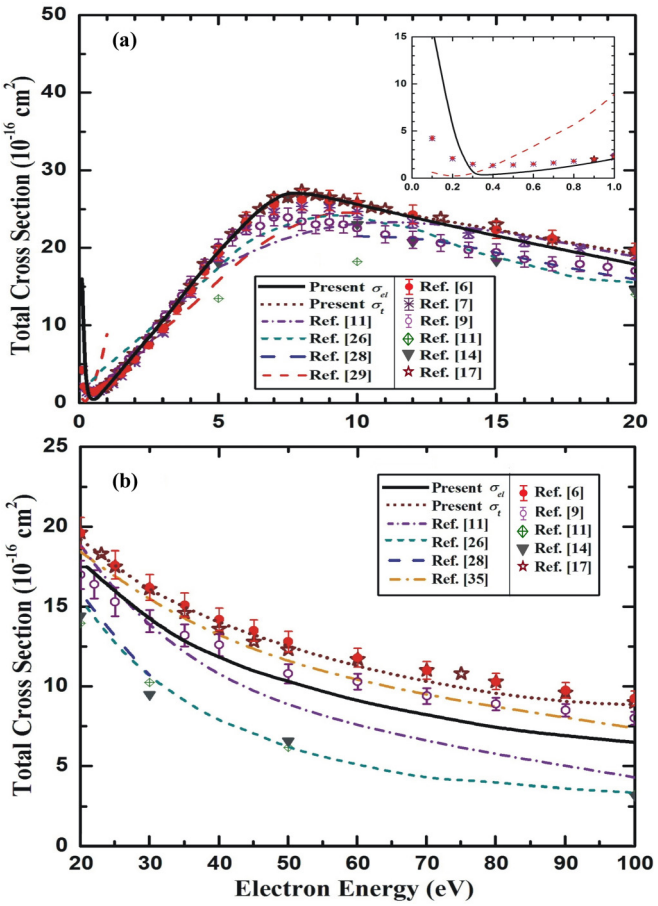

FIG. 2. Total cross sections for $e-CH_4$ scattering in the energy range (a) 0.1–20 eV and (b) 20–100 eV. Present results: Black solid line, σ_{el} results; wine short dotted line, σ_t results. Other calculations: Violet short dashed-dot line, Cho *et al.* [11]; dark cyan short dashed line, Vinodkumar *et al.* [26]; blue dashed line, Bettega *et al.* [28]; red dashed line, Bettega *et al.* [29]; orange dashed-dot line, Jain and Baluja [35]. Experimental data: Red filled circle, Song *et al.* [6]; violet cross with plus, Lohmann and Buckman [7]; purple hollow circle, Sueoka and Mori [9]; olive diamond with plus, Cho *et al.* [11]; dark gray inverted filled triangle, Boesten and Tanaka [14]; wine open star, Zecca *et al.* [17].

exchange and polarization interactions play an important role. Beyond 20 eV, the effect of both the exchange and polarization terms seems to be constant which is due to the fact that the correlation polarization potential is energy independent. The inset of Fig. 2(a) clearly shows that our σ_{el} results reproduce the RT minima at 0.35 eV (E_{RT}) which is in close agreement with the experimental measurements of Lohmann and Buckman [7] as well as the recommended values of Song *et al.* [6]. Appearance of a RT minimum is a very sensitive test for any theoretical model. This is one of the main merits of the present calculation. It is tempting to correlate the de Broglie wavelength of the electron energy of 0.35 eV where the RT minimum appears. It is an equivalent three-dimensional (3D) spherical potential well of radius (R_{sph}) which can be estimated by evaluating the de Broglie wavelength $\lambda_D = 2\pi/k$ where k is the wave number. Half of the λ_D (that introduces a phase shift of π rad in the scattering wave function) must fit in

TABLE I. Parameters for RT minimum for T_d molecules.

Target Molecule	α_o (a_0^3)	E_{RT} (eV)	R_{sph} (Å)	a_{sc} (Å)	σ_{sc} (Å^2)
CH_4	17.5 [35]	0.35	10.37	− 1.55	30.27
SiH_4	31.9 [49]	0.3	11.20	− 2.63	86.64
GeH_4	44.353 [41]	0.6	7.92	− 5.16	334.96

the radius of the spherical well potential. We obtain a value of 10.37 Å for CH_4. From modified effective range theory (MERT) we can estimate the scattering length $a_{sc} = (\pi/3)k\alpha_o$ where α_o is the polarizability of the target molecules. For CH_4, we obtain a value of −1.55 Å that yields a cross section at zero energy $\sigma_{sc} = 4\pi a_{sc}^2$ equal to 30.27 Å^2. A similar analysis for all three target molecules is summarized in Table I. Thereafter, in Fig. 2(a), we detect a shape resonance centered at 7.8 eV and the position of resonance is similar as found in the experimental results of Zecca *et al.* [17] as well as Song *et al.* [6]. After this energy the cross sections are decreasing and the trend is similar in the experimental as well as theoretical results. Up to 11 eV, both our σ_{el} and σ_t cross sections are similar to each other as the absorption potential becomes effective after threshold energy. It is clearly seen that the inclusion of the imaginary part significantly improves the results. The present σ_t results are in excellent agreement with the recommended values of Song *et al.* [6] in the entire energy range as well as the experimental results of Zecca *et al.* [17], whereas the measurements of Sueoka *et al.* [8] are lower by about 10%. In Fig. 2(b), σ_{el} and σ_t cross sections are presented in the energy range from 20 to 100 eV. Up to 60 eV, the present σ_t results are in excellent agreement with the results of Song *et al.* [6] as well as Zecca *et al.* [17]; thereafter the present σ_t results are slightly lower.

The momentum-transfer cross section is a signature of the backward scattering. This is an important parameter that appears in the Boltzmann equation and describes the electron distribution function. This is useful in the study of drift velocity of a swarm of electrons moving through a particular atomic or molecular medium. Keeping this in mind, the elastic momentum-transfer cross sections (σ_m) are calculated in the energy range 0.1–100 eV. These cross sections (σ_m) are presented in Figs. 3(a) and 3(b) in the energy region from 0.1 to 20 eV and from 20 to 100 eV, respectively. The present calculated σ_m results are compared with the experimental measurements [6,11,14,15] along with available theoretical calculations [11,28]. In this figure, it is noted that the present results agree well with Song *et al.* [6] in the entire energy range except at energies between 5 and 8 eV. The corresponding data below 1 eV are also shown in the inset of this figure. The inset of Fig. 3(a) clearly shows that our σ_m results reproduce the RT minima at 0.3 eV which are at a position similar to that of experimental measurements [15], as well as to that of Song *et al.* [6]. Further, Fig. 3(b) illustrates that the present σ_m results agree well with the experimental values.

B. Electron scattering from silane, SiH_4

In the case of the SiH_4 molecule, we have presented elastic DCSs on the same energies as those for the CH_4 molecule.

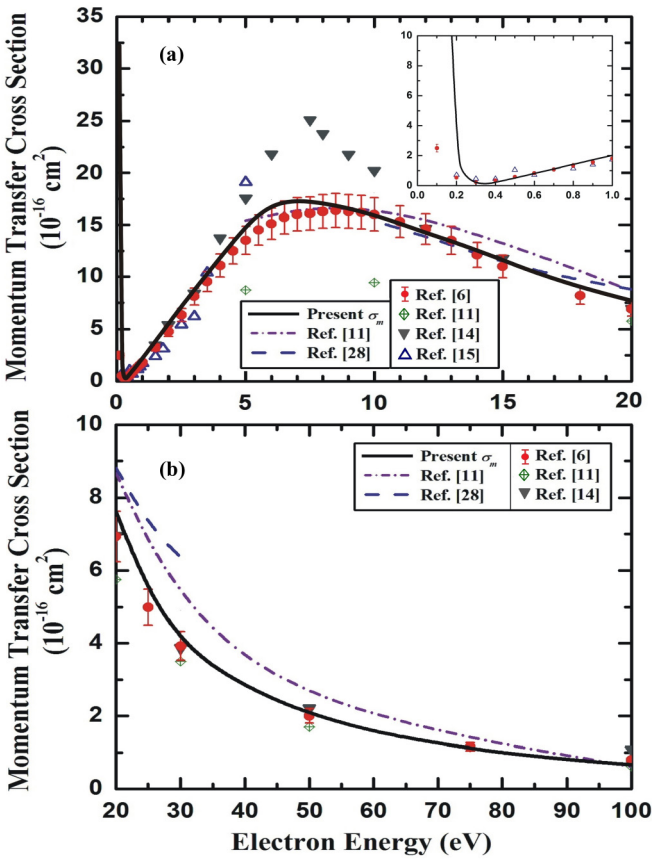

FIG. 3. Momentum-transfer cross sections for $e-CH_4$ scattering in the energy range (a) 0.1–20 eV and (b) 20–100 eV. Present results: Black solid line, elastic σ_m results. Other calculations: Violet short dashed-dot line, Cho *et al.* [11]; blue dashed line, Bettega *et al.* [28]. Experimental data: Red filled circle, Song *et al.* [6]; olive diamond with plus, Cho *et al.* [11]; dark gray inverted filled triangle, Boesten and Tanaka [14]; blue hollow triangle, Sohn *et al.* [15].

We have compared our DCS results with the measurements of Tanaka *et al.* [16] which are available for all these energies except at 30 eV. Likewise we have also compared our DCS results with the available calculations [16,28,29,31]. Our DCSs for the $e-SiH_4$ scattering system are shown in Figs. 4(a)–4(f). The calculated SMC values of Winstead and McKoy [31] apparently have better agreement with the experimental measurements of Tanaka *et al.* [16] than our calculation at 5 eV [see Fig. 4(a)]. This seems to be fortuitous as better agreement is expected at higher energies (>5 eV) as the effect of polarization becomes less significant. We may point out that SMC calculations have been done in the static-exchange approximation only, thereby neglecting polarization coupling. The overall energy dependence of SMC calculation for DCS is less satisfactory as compared to the present calculation with the experiment. We expect that the better agreement of our calculation is due to inclusion of the polarization potential along with inelastic coupling. Note that there exist two minima at 75° and 125° due to destructive interference of various partial waves at low energy. In Fig. 4(b), DCSs are plotted for an energy of 7.5 eV. The present calculations of DCS are in good agreement with measurements of Tanaka *et al.* [16] up to 60° but overestimate the measurements at lower scattering angle by about 20%. Thereafter between 90° and 120° there is excellent agreement between the present results and the measurements compared to the previous calculations [16,29,31]. We have displayed our DCS results at 10 eV in Fig. 4(c). The present calculations reproduce the experimental measurements very well in the entire angular region except at the forward scattering angles, i.e., below 30° where they overestimate the measurements by about 15% because of divergence of DCSs in forward scattering. This trend is continued for the other higher energies, 15 and 20 eV [see Figs. 4(d) and 4(e)]. As the energy increases the dip positions are shifted toward higher scattering angles. In Fig. 4(f), the present DCSs at 30 eV have been compared with the only available calculation of Bettega *et al.* [28] as there are no experimental data available at this energy.

Figures 5(a) and 5(b) exhibit the calculated σ_{el} and σ_t cross sections for the $e-SiH_4$ system along with experimental measurements [8,16,18,19] as well as theoretical calculations [26,28,29,31,35,37,42]. Figure 5(a) shows the present σ_{el} and σ_t cross sections in the energy range 0.1–20 eV. The corresponding data below 1 eV are also shown in the inset which clearly indicates that our σ_{el} results reproduce RT minima at 0.3 eV which is almost at a similar position as found in the measurements of Wan *et al.* [19]. At energy below 1 eV the present model produces very good results as compared to the results of Vinodkumar *et al.* [26] which are calculated by using QUANTEMOL-N formalism for low energy. Their [26] results completely disagree with the calculations and measurements of other researchers. Thereafter, we found a shape resonance centered at 2.9 eV. The position of shape resonance is the same as in the experimental results of Szmytkowski *et al.* [18]. Further, measurements and calculations decrease monotonically. Up to 9 eV, both our σ_{el} and σ_t results are similar to each other because the inelastic channels become active after threshold energy. It is clearly seen that the inclusion of the imaginary part after 9 eV significantly improves the results. In the entire energy region, the total cross sections reproduce the measurements with an excellent agreement. In Fig. 5(b) σ_{el} and σ_t cross sections are presented in the energy range 20–100 eV. Here the effect of inelastic channels is more noticeable which clearly shows that the inclusion of the imaginary part enables us to reproduce the experimental measurements of Szmytkowski *et al.* [18] in almost the entire energy range. The present results are also compared with the measurements of Zecca *et al.* [20] which are available above 75 eV and it is found that the present results are approximately 7% lower than their values [20].

In Fig. 6(a), the present σ_m results are compared with the experimental measurements [10,16,23] as well as the theoretical calculations [31,38,42] in the energy range up to 20 eV. The corresponding data below 1 eV are shown in the inset which shows that our σ_m results reproduce excellently the experimental measurements of Ohmori *et al.* [10] and we get RT minima at 0.3 eV which is at a similar position as obtained in their measurement. Thereafter is a shape resonance at around 4 eV and results agrees well with the measurements of Hayashi [23] in the entire energy region. The results of Ohmori *et al.* [10] are presented up to 1 eV. Figure 6(b) illustrates σ_m cross sections in the energy range 20–100 eV

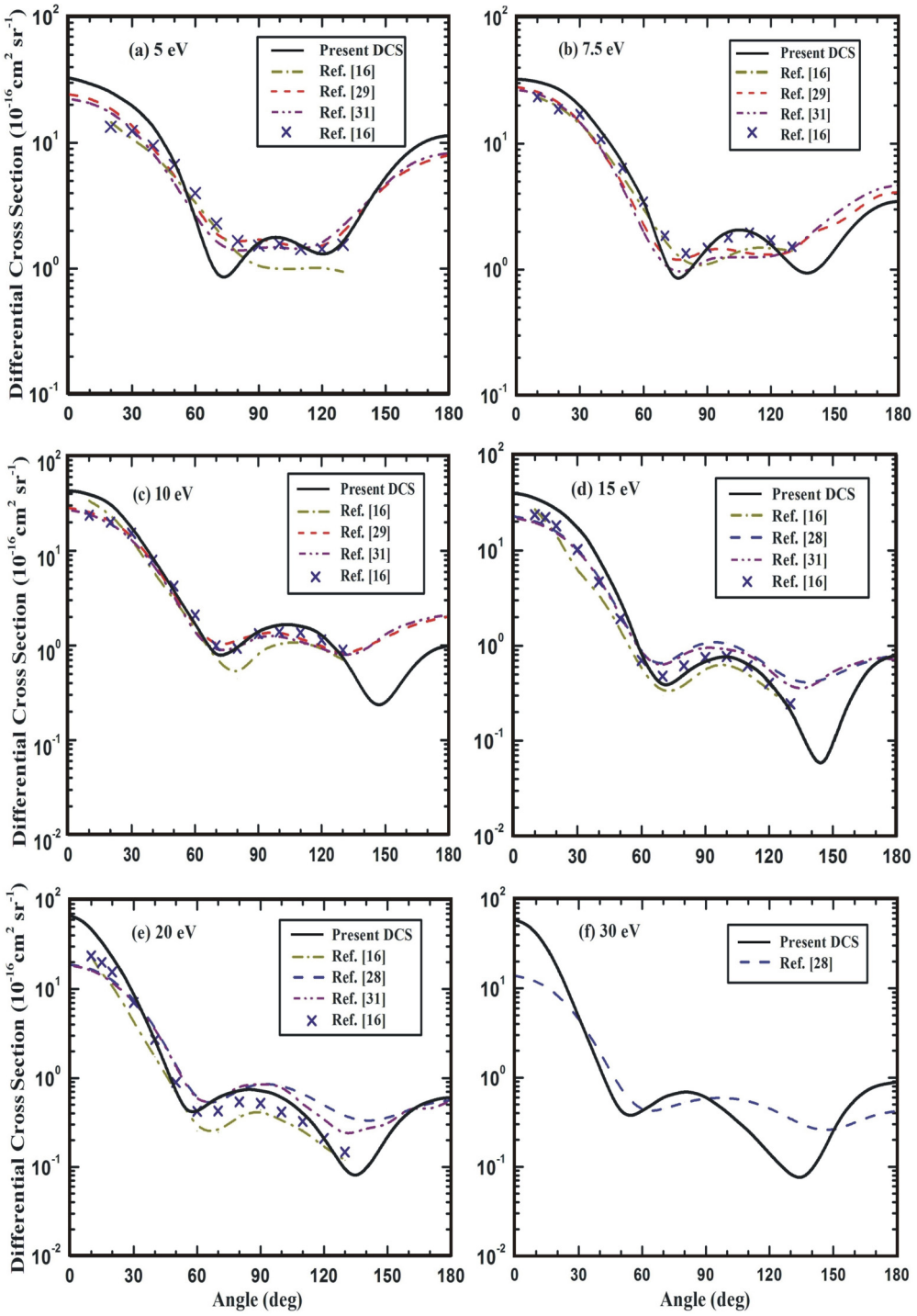

FIG. 4. Differential cross sections for $e-SiH_4$ scattering at energies (a) 5; (b) 7.5; (c) 10; (d) 15; (e) 20, and (f) 30 eV. Present results: Black solid line, elastic DCS. Other calculations: Dark yellow dashed-dot line, Tanaka *et al.* [16]; blue dashed line, Bettega *et al.* [28]; red dashed line, Bettega *et al.* [29]; purple dashed-dot-dot line, Winstead and McKoy [31]. Experimental data: Royal cross, Tanaka *et al.* [16].

along with other calculations [28,31,42] and the only available experimental results of Hayashi [23]. The present σ_m results agree very well with the measurements [23] up to 25 eV. Thereafter up to 70 eV, the present results are a bit higher than those of Hayashi [23] and about 5% lower than the calculations of Bettega *et al.* [28] which are available only up to 30 eV.

C. Electron scattering from germane, GeH_4

The elastic DCSs for GeH_4 molecules are shown in Figs. 7(a)–7(f) at similar energies as those for earlier molecules. Except at an energy of 30 eV, we have shown on each curve the measurement of Dillon *et al.* [24] as well as the calculation of Lee *et al.* [34] and Jain *et al.* [41]. The calculated DCSs of Bettega *et al.* [28,29] are also available

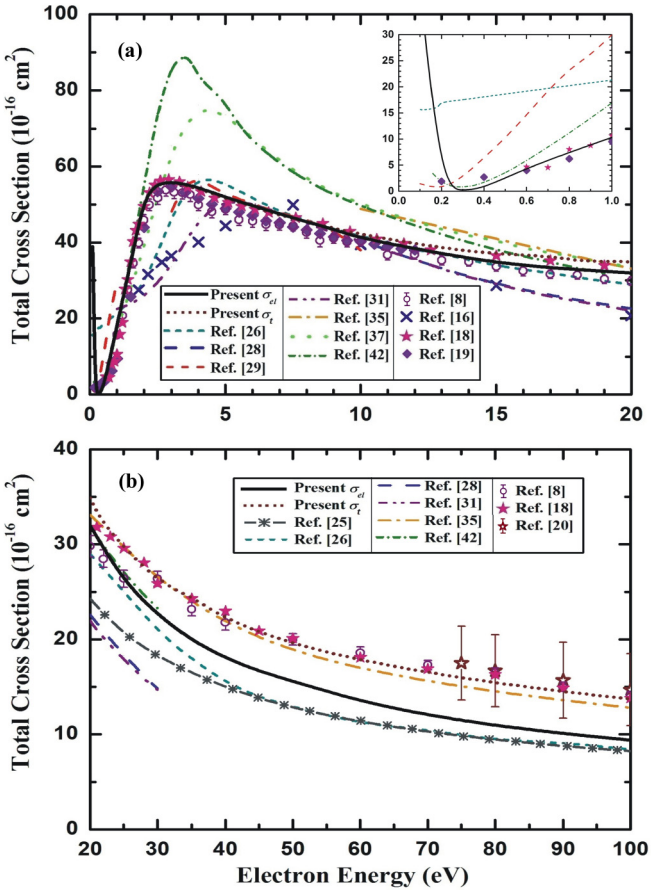

FIG. 5. Total cross sections for $e-SiH_4$ scattering in the energy range (a) 0.1–20 eV and (b) 20–100 eV. Present results: Black solid line, σ_{el} results; wine short dotted line, σ_t results. Other calculations: Dark gray dashed-cross line, Mozejko *et al.* [25]; dark cyan short dashed line, Vinodkumar *et al.* [26]; blue dashed line, Bettega *et al.* [28]; red dashed line, Bettega *et al.* [29]; purple dashed-dot-dot line, Winstead and McKoy [31]; orange dashed-dot line, Jain and Baluja [35]; green dotted line, Yuan [37]; olive short dashed-dot line, Jain *et al.* [42]. Experimental data: Purple hollow circle, Sueoka *et al.* [8]; royal cross, Tanaka *et al.* [16]; pink filled star, Szmytkowski *et al.* [18]; violet filled diamond, Wan *et al.* [19]; wine hollow star, Zecca *et al.* [20].

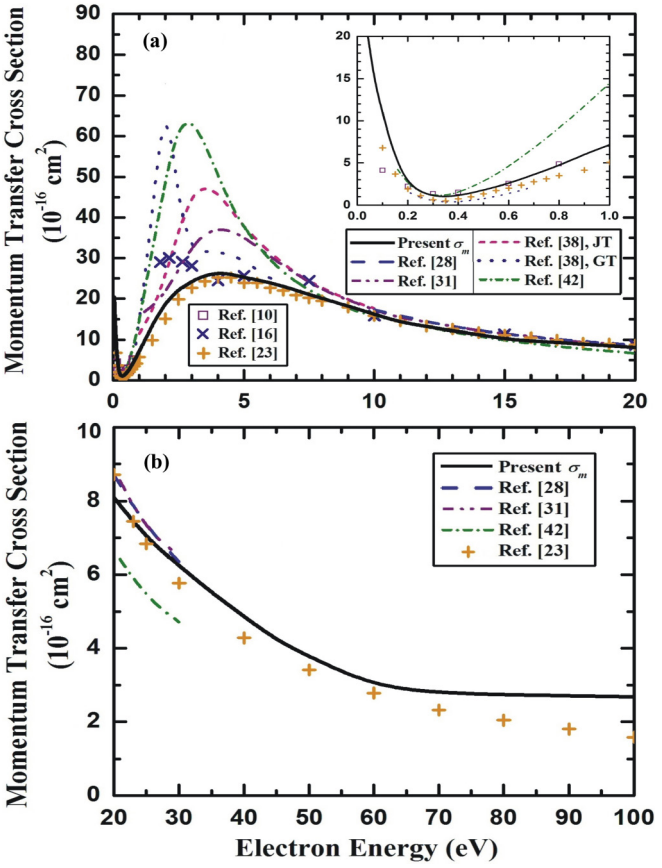

FIG. 6. Momentum-transfer cross sections for $e-SiH_4$ scattering in the energy range (a) 0.1–20 eV and (b) 20–100 eV. Present results: Black solid line, elastic σ_m results. Other calculations: Blue dashed line, Bettega *et al.* [28]; purple dashed-dot-dot line, Winstead and McKoy [31]; pink short dashed line, Jain and Thompson (JT) [38]; royal dotted line, Jain and Thompson (GT) [38]; olive short dashed-dot line, Jain *et al.* [42]. Experimental data: Purple hollow square, Ohmori *et al.* [10]; royal cross, Tanaka *et al.* [16]; orange plus, Hayashi [23].

at the selected energies; therefore these are also included here. At an incident energy of 5 eV [Fig. 7(a)], the present calculated DCSs are in better agreement with the measurements of Dillon *et al.* [24] at angles between 30° and 100° in comparison with other calculations. The only significant difference between the present calculated and the experimental DCSs is observed at around a scattering angle of 120°, where our DCS curve displays a dip in contrast to a less pronounced experimental dip. This may be due to the fact that below 10 eV, rotationally inelastic channels are insignificant. In the present calculation, below the electronic excitation threshold energy (which is 7.5 eV for the GeH_4 molecule), the imaginary part [V_{abs}] of the optical potential does not play any role. A similar trend for the DCS is seen for the next higher energies, i.e., 7.5 and 10 eV [see Figs. 7(b) and 7(c), respectively]. As the energy increases, the dip positions are shifted toward higher scattering angles. In Fig. 7(d), DCSs are plotted at 15 eV. The present DCSs exhibit two dips, interspersed with a shallow hump. These DCSs are in good agreement with the measurements of Dillon *et al.* [24] in the entire angular region. The inclusion of the absorption potential reduces the elastic differential cross sections by a significant amount, particularly at middle angles, whereas other calculations differ considerably. Similar behavior of the DCS curve is observed for the next higher energy, i.e., 20 eV [see Fig. 7(e)]. In Fig. 7(f) DCSs are shown at an energy of 30 eV. At this energy, the single calculation of Bettega *et al.* [28] is available for comparison. The shape of the present curve is almost the same as that of Bettega *et al.* [28]. There is a need of experimental progress for $e-GeH_4$ collisions for the assessment of the present results.

Figures 8(a) and 8(b) exhibit the present calculated σ_{el} and σ_t cross sections which are compared with the experimental measurements [21,22,24] as well as theoretical calculation [28,29,34,41]. Figure 8(a) shows the cross sections in the energy range 0.1–20 eV. The corresponding data below 1 eV are also shown in the inset of this figure. Note that below the threshold energy for the first electronic excitation the effect of

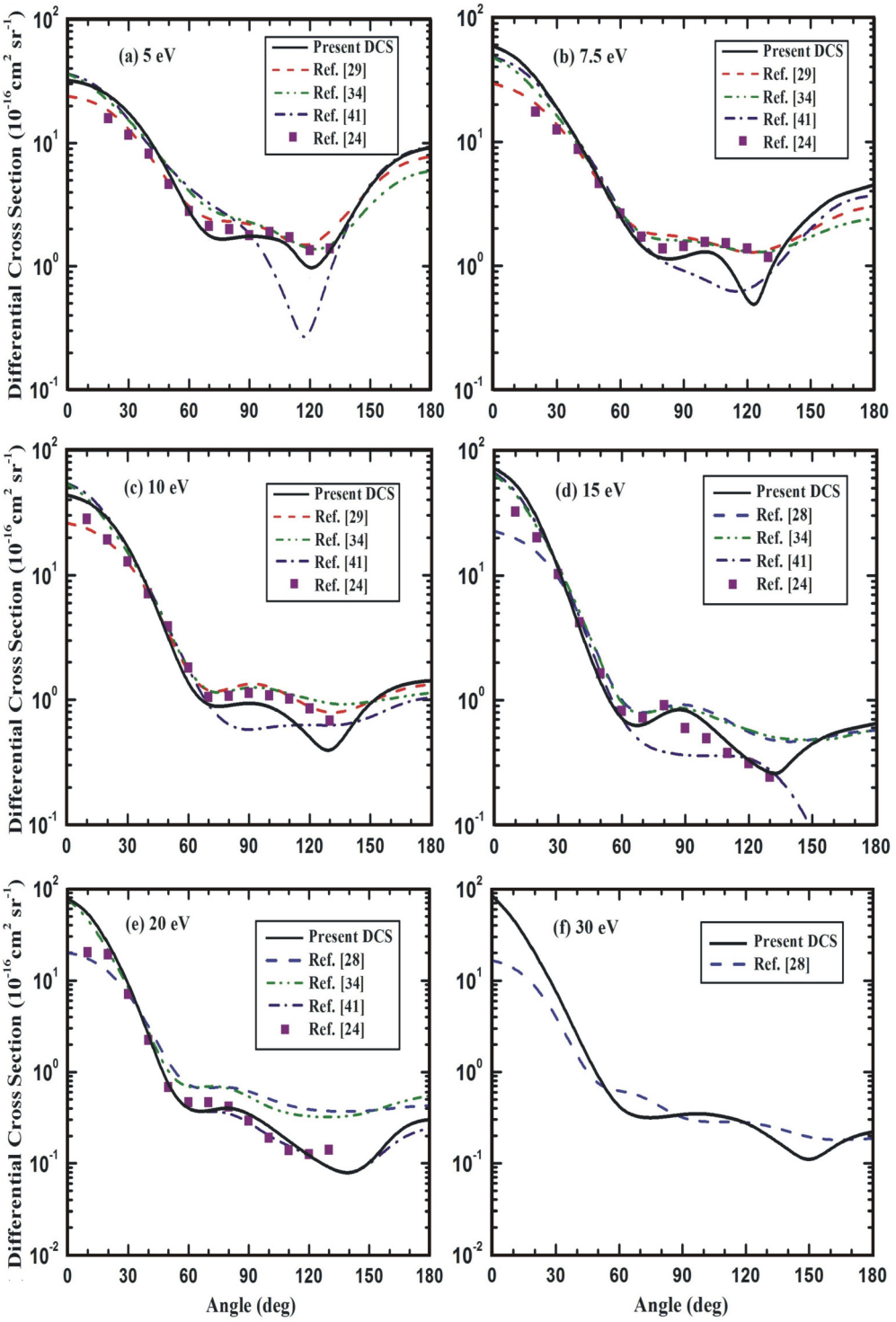

FIG. 7. Differential cross sections for $e-GeH_4$ scattering at energies (a) 5; (b) 7.5; (c) 10; (d) 15; (e) 20, and (f) 30 eV. Present results: Black solid line, elastic DCS. Other calculations: Blue dashed line, Bettega *et al.* [28]; red dashed line, Bettega *et al.* [29]; olive dashed-dot-dot line, Lee *et al.* [34]; navy dashed-dot line, Jain *et al.* [41]. Experimental data: Purple filled square, Dillon *et al.* [24].

the absorption potential is negligible. Therefore, in the case of the GeH_4 molecule up to 7.5 eV, the cross sections are elastic and thereafter both σ_{el} and σ_t cross sections are available for comparison. The inset of Fig. 8(a) clearly shows that the RT minimum appears around 0.6 eV which is at a similar position as calculated by Lee *et al.* [34]. All results indicate the presence of a shape resonance. In particular, our calculated resonance location is around 3.8 eV, which agrees well with the location given by Mozejko *et al.* [22] but its magnitude is slightly higher (i.e., about 3.5%) than the experimental data. Up to 4 eV, the present calculated results are in good agreement with the measurements [22]. It is noticed that most of the

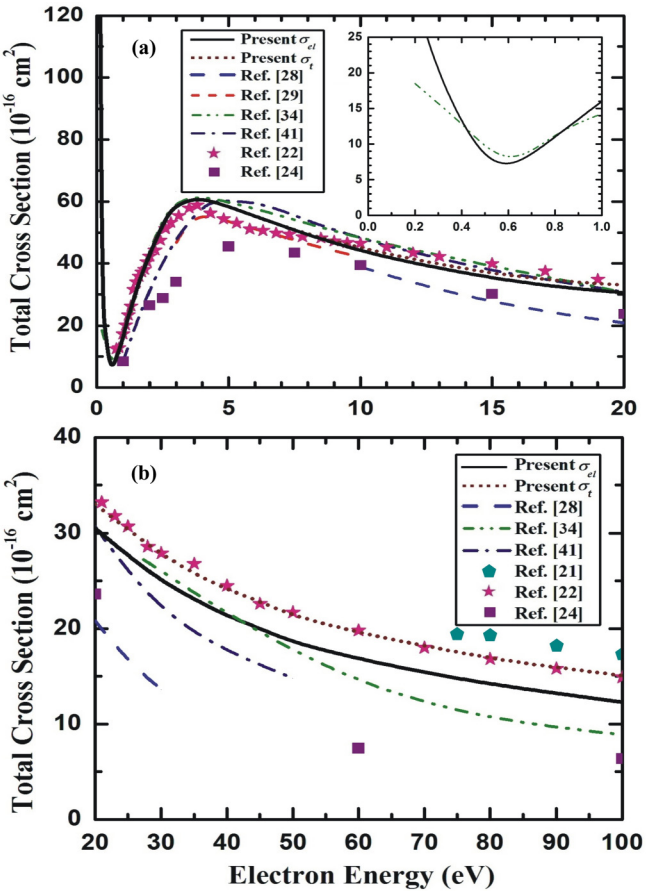

FIG. 8. Total cross sections for $e-GeH_4$ scattering in the energy range (a) 0.1–20 eV and (b) 20–100 eV. Present results: Black solid line, σ_{el} results; wine short dotted line, σ_t results. Other calculations: Blue dashed line, Bettega *et al.* [28]; red dashed line, Bettega *et al.* [29]; olive dashed-dot-dot line, Lee *et al.* [34]; navy dashed-dot line, Jain *et al.* [41]. Experimental data: Dark cyan filled pentagon, Karwasz [21]; pink filled star, Mozejko *et al.* [22]; purple filled square, Dillon *et al.* [24].

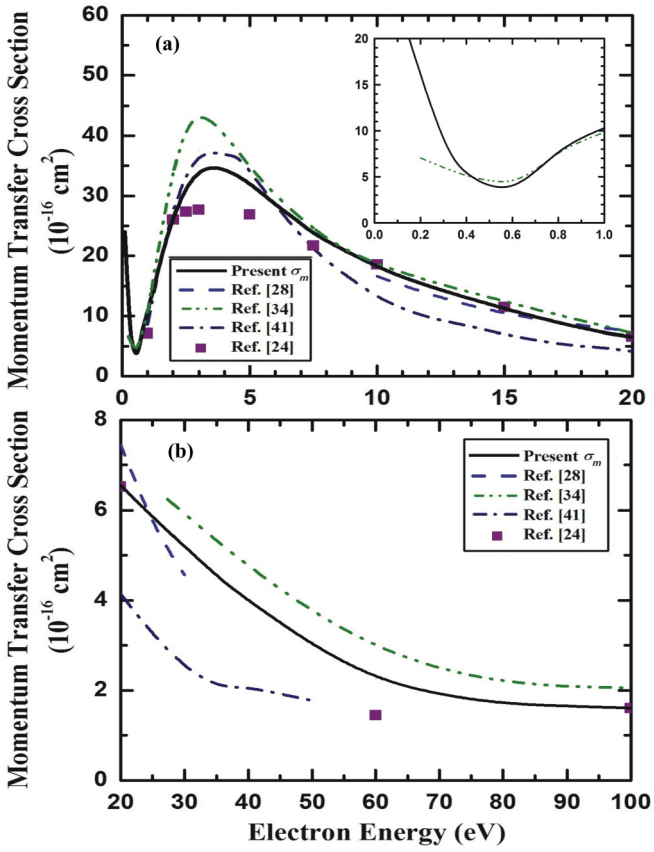

FIG. 9. Momentum-transfer cross sections for $e-GeH_4$ scattering in the energy range (a) 0.1–20 eV and (b) 20–100 eV. Present results: Black solid line, elastic σ_m results. Other calculations: Blue dashed line, Bettega *et al.* [28]; olive dashed-dot-dot line, Lee *et al.* [34], navy dashed-dot line, Jain *et al.* [41]. Experimental data: Purple filled square, Dillon *et al.* [24].

calculations including the present one differ significantly from the measurements of Mozejko *et al.* [22] in the energy region 4–7 eV. The present calculated σ_{el} cross sections are about 10% higher. However, the calculation of Bettega *et al.* [29] agrees well with these experimental data in this region. Beyond 8 eV (i.e., above threshold energy), inelastic channels become effective which is clearly observed from the figure. The present calculated σ_t cross sections agree well with the measurements compared to other calculations. These are about 10% lower than the measurements [22] in the energy region 8–20 eV. Figure 8(b) displays cross sections in the energy region between 20 and 100 eV. In this energy region, we present both our σ_{el} and σ_t cross sections along with the measurements [21,22,24]. Theoretical calculations of Bettega *et al.* [28] up to 30 eV, Lee *et al.* [34], and Jain *et al.* [41] up to 50 eV are also available for comparison. It is clear that with increase in incident energy inclusion of the absorption potential considerably improves the results compared to the other calculations with respect to the measurements of Mozejko *et al.* [22].

Finally, σ_m cross sections are presented in Figs. 9(a) and 9(b) in the energy region from 0.1 to 20 eV and from 20 to 100 eV, respectively. These are also compared with the calculations of Bettega *et al.* [28] up to 30 eV, Lee *et al.* [34], and Jain *et al.* [41] up to 50 eV, and measurements of Dillon *et al.* [24]. The σ_m cross sections below 1 eV are displayed in the inset of Fig. 9(a). Experimental observations are not available in this low-energy region. Therefore calculated results are compared with the static-exchange plus correlation polarization calculation of Lee *et al.* [34]. Both calculations demonstrate a RT minimum at around 0.6 eV. Figure 9(a) shows the present σ_m cross sections along with the available calculations and measurement. All the calculations exhibit a shape resonance around 3 eV but with a different magnitude. Our σ_m cross sections are closest to the experimental values of Dillon *et al.* [24]. Beyond 8 eV, the present σ_m cross sections are in good agreement with the experiments compared to other calculations. Beyond 20 eV, σ_m cross sections are shown in Fig. 9(b). It is clear from the figure that all cross sections decrease monotonically with the increasing incident electron energy.

IV. CONCLUSIONS

In this paper we have presented elastic DCSs, integral, and momentum-transfer cross sections, along with total (elastic plus inelastic) cross sections for scattering of electrons with

tetrahedral molecules (CH_4, SiH_4, GeH_4) at energies 0.1–100 eV. A spherical complex optical potential is generated for these nonpolar molecules. The present calculated cross sections are compared with the available calculations and measurements. The agreement between the present calculations and experiments is reasonably good at all impact energies considered here. Our main conclusions are as follows:

(1) The present model is able to predict the quantitative features of the scattering parameters such as the RT minimum at around 0.35 eV for CH_4, 0.3 eV for SiH_4, and 0.6 eV for GeH_4 and shape resonance structure at around 7.8 eV for CH_4, 2.9 eV for SiH_4, and 3.8 eV for GeH_4 as observed in other theoretical calculation or experimental measurement.

(2) We have studied the correlation of energy when the RT minimum occurs with an equivalent 3D spherical well and scattering length.

(3) The inclusion of the imaginary part considerably improves the results. Our calculated σ_t results are in very good agreement with the experimental measurements compared to other theoretical results.

(4) The anisotropy of the molecular field poses no serious problem, since for these symmetrical molecules, the first two multiple moments (i.e., dipole and quadrupole) are zero.

Finally, there is a need of experimental progress for $e-GeH_4$ collisions for the assessment of the present results, especially on the total and momentum-transfer cross sections in the low-energy region. Our calculated results may provide a benchmark for future experimental measurements.

ACKNOWLEDGMENTS

M.K. gratefully acknowledges the financial support from University Grants Commission, New Delhi, India, under Grant No. F1-17.1/2011/MANF-SIK-HAR-1601. G.K. is thankful for financial support from the Science and Engineering Research Board, Department of Science and Technology, New Delhi, India (Project No. PDF/2015/000065) under which a part of this work was done.

[1] M. Martinez-Canales, A. R. Oganov, Y. Ma, Y. Yan, A. O. Lyakhov, and A. Bergara, Phys. Rev. Lett. **102**, 087005 (2009).
[2] G. Gao, A. R. Oganov, A. Bergara, M. Martinez-Canales, T. Cui, T. Iitaka, Y. Ma, and G. Zou, Phys. Rev. Lett. **101**, 107002 (2008).
[3] E. Woelk, D. V. Shenai-Khatkhate, R. L. DiCarlo, Jr., A. Amamchyan, M. B. Power, B. Lamare, G. Beaudoin, and I. Sagnes, J. Cryst. Growth **287**, 684 (2006).
[4] A. Ohki, T. Ohmi, J. Date, and T. Kijima, J. Electrochem. Soc. **145**, 3560 (1998).
[5] F. Fujimoto, A. Ootuka, K. Komaki, Y. Iwata, I. Yamane, H. Yamashita, Y. Hashimoto, Y. Tawada, K. Nishimura, H. Okamoto, and Y. Hamakawa, Jpn. J. Appl. Phys. **23**, 810 (1984).
[6] M.-Y. Song, J.-S. Yoon, H. Cho, Y. Itikawa, G. P. Karwasz, V. Kokoouline, Y. Nakamura, and J. Tennyson, J. Phys. Chem. Ref. Data **44**, 023101 (2015).
[7] B. Lohmann and S. J. Buckman, J. Phys. B: At. Mol. Phys. **19**, 2565 (1986).
[8] O. Sueoka, S. Mori, and A. Hamada, J. Phys. B: At., Mol. Opt. Phys. **27**, 1453 (1994).
[9] O. Sueoka and S. Mori, J. Phys. B: At. Mol. Phys. **19**, 4035 (1986).
[10] Y. Ohmori, M. Shimozuma, and H. Tagashira, J. Phys. D: Appl. Phys. **19**, 1029 (1986).
[11] H. Cho, Y. S. Park, E. A. y. Castro, G. L. C. de Souza, I. Iga, L. E. Machado, L. M. Brescansin, and M.-T. Lee, J. Phys. B: At., Mol. Opt. Phys. **41**, 045203 (2008).
[12] P. J. Curry, W. R. Newell, and A. C. H. Smith, J. Phys. B: At. Mol. Phys. **18**, 2303 (1985).
[13] H. Tanaka, T. Okada, L. Boesten, T. Suzuki, T. Yamamoto, and M. Kubo, J. Phys. B: At. Mol. Phys. **15**, 3305 (1982).
[14] L. Boesten and H. Tanaka, J. Phys. B: At., Mol. Opt. Phys. **24**, 821 (1991).
[15] W. Sohn, K.-H. Kochem, K.-M. Scheuerlein, K. Jung, and H. Ehrhardt, J. Phys. B: At. Mol. Phys. **19**, 3625 (1986).
[16] H. Tanaka, L. Boesten, H. Sato, M. Kimura, M. A. Dillon, and D. Spence, J. Phys. B: At., Mol. Opt. Phys. **23**, 577 (1990).
[17] A. Zecca, G. Karwasz, R. S. Brusa, and Cz. Szmytkowski, J. Phys. B: At., Mol. Opt. Phys. **24**, 2747 (1991).
[18] Cz. Szmytkowski, P. Mozejko, and G. Kasperski, J. Phys. B: At., Mol. Opt. Phys. **30**, 4363 (1997).
[19] H.-X. Wan, J. H. Moore, and J. A. Tossell, J. Chem. Phys. **91**, 7340 (1989).
[20] A. Zecca, G. P. Karwasz, and R. S. Brusa, Phys. Rev. A **45**, 2777 (1992).
[21] G. P. Karwasz, J. Phys. B: At., Mol. Opt. Phys. **28**, 1301 (1995).
[22] P. Mozejko, G. Kasperski, and Cz. Szmytkowski, J. Phys. B: At., Mol. Opt. Phys. **29**, L571 (1996).
[23] M. Hayashi, *Swarm Studies and Inelastic Electron-Molecule Collisions* (Springer-Verlag, New York, 1985), p. 167.
[24] M. A. Dillon, L. Boesten, H. Tanaka, M. Kimura, and H. Sato, J. Phys. B: At., Mol. Opt Phys. **26**, 3147 (1993).
[25] P. Mozejko, B. Zywicka-Mozejko, and Cz. Szmytkowski, Nucl. Instrum. Methods Phys. Res., Sect. B **196**, 245 (2002).
[26] M. Vinodkumar, C. G. Limbachiya, K. N. Joshipura, and N. J. Mason, Eur. Phys. J. D **61**, 579 (2011).
[27] B. M. Nestmann, K. Pfingst, and S. D. Peyerimhoff, J. Phys. B: At., Mol. Opt. Phys. **27**, 2297 (1994).
[28] M. H. F. Bettega, A. P. P. Natalense, M. A. P. Lima, and L. G. Ferreira, J. Chem. Phys. **103**, 10566 (1995).
[29] M. H. F. Bettega, M. T. do N. Varella, and M. A. P. Lima, Phys. Rev. A **68**, 012706 (2003).
[30] C. Winstead, P. G. Hipes, M. A. P. Lima, and V. McKoy, J. Chem. Phys. **94**, 5455 (1991).
[31] C. Winstead and V. McKoy, Phys. Rev. A **42**, 5357 (1990).
[32] M. A. P. Lima, T. L. Gibson, W. M. Huo, and V. McKoy, Phys. Rev. A **32**, 2696 (1985).
[33] M. A. P. Lima, K. Watari, and V. McKoy, Phys. Rev. A **39**, 4312 (1989).

[34] M.-T. Lee, L. M. Brescansin, and L. E. Machado, Phys. Rev. A **59**, 1208 (1999).
[35] A. Jain and K. L. Baluja, Phys. Rev. A **45**, 202 (1992).
[36] A. Jain, J. Chem. Phys. **78**, 6579 (1983).
[37] J. Yuan, J. Phys. B: At., Mol. Opt. Phys. **21**, 2737 (1988).
[38] A. Jain and D. G. Thompson, J. Phys. B: At. Mol. Phys. **20**, 2861 (1987).
[39] A. Jain, Phys. Rev. A **34**, 3707 (1986); J. Phys. B: At. Mol. Phys. **19**, L807 (1986).
[40] A. Jain, J. Chem. Phys. **86**, 1289 (1987).
[41] A. Jain, K. L. Baluja, V. Di Martino, and F. A. Gianturco, Chem. Phys. Lett. **183**, 34 (1991).
[42] A. K. Jain, A. N. Tripathi, and A. Jain, J. Phys. B: At. Mol. Phys. **20**, L389 (1987).
[43] G. Kaur, A. K. Jain, H. Mohan, P. S. Singh, S. Sharma, and A. N. Tripathi, Phys. Rev. A **91**, 022702 (2015).
[44] F. A. Gianturco and A. Jain, Phys. Rep. **143**, 347 (1986).
[45] J. K. O'Connell and N. F. Lane, Phys. Rev. A **27**, 1893 (1983).
[46] N. T. Padial and D. W. Norcross, Phys. Rev. A **29**, 1590 (1984).
[47] F. A. Gianturco and S. Scialla, J. Phys. B: At. Mol. Phys. **20**, 3171 (1987).
[48] M. G. Curtis and I. C. Walker, J. Chem. Soc. Faraday Trans. 2, **85**, 659 (1989).
[49] G. Cooper, G. R. Burton, W. F. Chan, and C. E. Brion, Chem. Phys. **196**, 293 (1995).
[50] F. A. Gianturco and D. G. Thompson, Chem. Phys. **14**, 111 (1976).
[51] F. A. Gianturco, A. Jain, and L. C. Pantano, J. Phys. B: At. Mol. Phys. **20**, 571 (1987).
[52] F. Blanco and G. Garcia, Phys. Lett. A **255**, 147 (1999).
[53] F. Calagero, *Variable Phase Approach to Potential Scattering* (Academic, New York, 1967).